Mitochondrial Respiration in Outer Retina Contributes to Light-Evoked Increase in Hydration In Vivo

Bruce A. Berkowitz,[1] Robert H. Podolsky,[2] Haohua Qian,[3] Yichao Li,[3] Ke Jiang,[4] Jacob Nellissery,[4] Anand Swaroop,[4] and Robin Roberts[1]

[1]Department of Ophthalmology, Visual and Anatomical Sciences, Wayne State University School of Medicine, Detroit, Michigan, United States
[2]Beaumont Research Institute, Beaumont Health, Royal Oak, Michigan, United States
[3]Visual Function Core National Eye Institute, National Institutes of Health, Bethesda, Maryland, United States
[4]Neurobiology-Neurodegeneration and Repair Laboratory, National Eye Institute, National Institutes of Health, Bethesda, Maryland, United States

Correspondence: Bruce A. Berkowitz, Department of Ophthalmology, Visual and Anatomical Sciences, Wayne State University School of Medicine, 540 East Canfield, Detroit, MI 48201, USA; baberko@med.wayne.edu.

Submitted: September 6, 2018
Accepted: October 27, 2018

Citation: Berkowitz BA, Podolsky RH, Qian H, et al. Mitochondrial respiration in outer retina contributes to light-evoked increase in hydration in vivo. *Invest Ophthalmol Vis Sci*. 2018;59:5957–5964. https://doi.org/10.1167/iovs.18-25682

Purpose. To test the hypothesis that mitochondrial respiration contributes to local changes in hydration involved in phototransduction-driven expansion of outer retina, as measured by structural responses on optical coherence tomography (OCT) and diffusion magnetic resonance imaging (MRI).

Methods. Oxygen consumption rate and mitochondrial reserve capacity of freshly isolated C57BL/6 and 129S6/SvEvTac mouse retina were measured using a Seahorse Extracellular Flux Analyzer. Light-stimulated outer retina layer water content was determined by proton density MRI, structure and thickness by ultrahigh-resolution OCT, and water mobility by diffusion MRI.

Results. Compared with C57BL/6 mice, 129S6/SvEvTac retina demonstrated a less robust mitochondrial respiratory basal level, with a higher reserve capacity and lower oxygen consumption in the light, suggesting a relatively lower production of water. C57BL/6 mice showed a light-triggered surge in water content of outer retina in vivo as well as an increase in hyporeflective bands, thickness, and water mobility. In contrast, light did not evoke augmented hydration in this region or an increase in hyporeflective bands or water mobility in the 129S6/SvEvTac outer retina. Nonetheless, we observed a significant but small increase in outer retinal thickness.

Conclusions. These studies suggest that respiratory-controlled hydration in healthy retina is linked with a localized light-evoked expansion of the posterior retina in vivo and may serve as a useful biomarker of the function of photoreceptor/retinal pigment epithelium complex.

Keywords: mitochondria, genetics, functional imaging, photoreceptor, water content

Sight-threatening disease of photoreceptor cells potentiate a substantial reduction in a person's quality of life, with an increased risk of falls, an important predictive factor of long-term survival.[1] Many photoreceptor diseases remain with inadequate or no therapies. One major reason for this limited progress has been the lack of high spatial resolution, noninvasive imaging of the morphology and function of photoreceptors. A conventional measure of photoreceptor physiology in vivo is electroretinography. However, the electroretinographic response is an integrated signal over the entire retina, and to a degree from different retinal layers, making it difficult to compare to localized structural changes, as measured by optical coherence tomography (OCT, the modality of choice for high spatial resolution imaging of photoreceptor anatomy in vivo). An alternative approach is to noninvasively measure aspects of focal photoreceptor cell subcompartment function by using high-resolution magnetic resonance imaging (MRI) and compare the results to OCT data.[2] At present, the wide availability of OCT in the clinic is motivating work to encode information about photoreceptor function into OCT images.

One important aspect of photoreceptor function is the light-stimulated expansion of outer retina volume. Such a response was first measured by microelectrodes in frog and chick retina ex vivo, and in vivo in cat retina, by diffusion MRI in mice and rats, and more recently by ultrahigh-resolution OCT in mice and people.[3–11] These studies imply, but do not establish, that outer retina (i.e., the photoreceptor/retinal pigment epithelium [RPE] complex) hydration is dynamically linked with its function and associated energy ecosystem. The health of photoreceptor cells is dependent on adequate hydration in order to regulate local ion and metabolite content, the composition of the interphotoreceptor matrix, and retinal adhesiveness to the RPE.[8,9,12,13]

Here, we test the hypothesis that mitochondrial respiration contributes to local changes in hydration involved in the phototransduction-driven expansion of the outer retina, as measured by structural responses on OCT and diffusion MRI.[3–7,14] We compared C57BL/6 and 129S6/SvEvTac mice, two strains with different RPE65 variants regulating distinct outer retina reactions to light; different expressions of functional *DISC1*, a regulator of an electron transport chain, monoamine oxidase, and Ca^{2+} activity, located in the basal body

Copyright 2018 The Authors

This work is licensed under a Creative Commons Attribution-NonCommercial-NoDerivatives 4.0 International License.

Downloaded from iovs.arvojournals.org on 04/21/2021

complex of the apical region of the mitochondria-rich inner segment;[15] and different photoreceptor histopathology outcomes to similar oxidative stress-inducing insults.[16–22] Together, these strain differences suggest distinct energy ecosystems in their outer retina. Photoreceptors account over 70% of cell populations and are the largest consumer of oxygen in the retina. Oxygen consumption is directly proportional to water production. These considerations imply a differential posterior retinal hydration status between the two strains, a hypothesis tested herein.

In this study, we first compared C57BL/6 and 129S6/SvEvTac retinal oxygen consumption rate (OCR) and mitochondrial maximum reserve capacity (MRC) ex vivo, which are two important indices of activity/efficiency of mitochondria function.[23,24] Next, we associated these strain-specific respiratory indices to in vivo light-evoked responses in posterior retina water content (proton density MRI), layer thickness (ultrahigh-resolution OCT), and water mobility (diffusion MRI).

Materials and Methods

All animals were treated in accordance with the National Institutes of Health Guide for the Care and Use of Laboratory Animals, the Association for Research in Vision and Ophthalmology Statement for the Use of Animals in Ophthalmic and Vision Research, and Institutional Animal and Care Use Committee authorizations at Wayne State University and National Eye Institute. We used male 2- to 3-month-old C57BL/6 (Jackson Labs, Bar Harbor, ME, USA) and 129S6/SvEvTac (Taconic Labs, Rensselaer, NY, USA) mice. Animals were housed and maintained under 12 hour:12 hour light:dark cycle laboratory lighting, unless otherwise noted. The exact number of mice used in each experimental condition is given in the figure legends. The sample sizes used for each experimental condition are based on our previous experience with each technique.[4,5,23,25]

Data Collection and Analysis

OCR and MRC. OCR of retinal punches was performed ex vivo according to the published protocol.[23] Briefly, three punches of 1-mm diameter equidistant from the optic nerve head (ONH) were taken from each retina for the measurement. Ames' buffer (120 mM NaCl) containing 10 mM HEPES (pH 7.35) was used in the assay. The mitochondrial uncoupler (2-fluorophenyl)(6-[(2-fluorophenyl)amino](1,2,5-oxadiazolo[3,4-e]pyrazin-5-yl))amine (BAM15; Timtec, Newark, DE, USA) and complex I inhibitor rotenone were used at a final concentration of 5 μM and 1 μM, respectively. Raw OCR values were computed by the Seahorse KSV algorithm. Nonmitochondrial respiration, which is the residual reading obtained after the addition of rotenone, was subtracted from all points.[26] Basal OCR was taken at the last point before BAM15 addition, and the highest value from uncoupled points was used as maximal OCR. All OCR values were normalized to cytochrome *a* quantity in retinal punch. MRC was calculated as 1 − (basal OCR/maximal OCR).

Ultrahigh-Resolution OCT. The procedure used for OCT imaging of mouse retina followed a published protocol.[5,27] Briefly, after mice were anesthetized with ketamine (100 mg/kg) and xylazine (6 mg/kg), retina OCT images were captured with Envisu UHR2200 (Bioptigen, Durham, NC, USA). The mouse eye was positioned with the ONH in the center of the OCT scan. Full field volume scans (1.4 mm × 1.4 mm at 1000 A-scan × 100 B-scan × 5) and two radial scans (at horizontal and vertical position and averaged 40 times) were captured. Mice retina were first imaged after ∼20 minutes of adaptation to room light (500 lux) in the procedure room under standard illumination conditions, and again in darkness after overnight dark adaptation. Averaged radial scan images were used for retinal thickness measurement. For each eye, measurements were performed on 4 spots (450 μm from center of ONH at both horizontal and vertical directions) by using the vendor-provided Reader program (Bioptigen), and an averaged number was used as the measurement for the eye. Outer retina length was measured from the outer limiting membrane to the RPE-choroid boundary.

MRI. The mouse preparation for all of the high-resolution MRI procedures is well established in our laboratory.[4] All animals were maintained in darkness for at least 16 hours before and during the dark phase of the MRI examination. High-resolution MRI data were acquired on a 7 T system (ClinScan; Bruker, Billerica, MA, USA) using a receive-only surface coil (1.0 cm diameter) centered on the left eye. The end of a fiber optic bundle was attached to a light source (Mark II Light Source; Prescott's, Inc., Monument, CO, USA) placed caudal to the eye, projecting at a white screen ∼1 cm from the eye, similar to that previously described.[3] We exposed the eye to 0 (i.e., dark) or ∼500 lux (confirmed outside the magnet using a Traceable Dual-Range Light Meter; (Control Company, Friendswood, TX, USA) placed against a 1-cm diameter aperture; measured this way the room lighting is ∼300 lux. Aside from the fiber optic light source, all lights in the MRI room were off. In all groups, immediately before the MRI experiment, animals were anesthetized with urethane (36% solution intraperitoneally; 0.083 ml/20 g animal weight, prepared fresh daily; Sigma-Aldrich Corp., St. Louis, MO, USA) and treated topically with 1% atropine to ensure dilation of the iris during light exposure, followed by 2% lidocaine to reduce eye motion and ensure continuous lubrication for the eye.

As previously detailed, retinal thicknesses (in μm) were objectively determined using the "half-height method" wherein a border is determined via a computer algorithm based on the crossing point at the midpoint between the local minimum and maximum, as detailed elsewhere.[28,29] The distance between two neighboring crossing points thus represents an objectively defined retinal thickness. 1/T1 profiles in each mouse were then normalized with 0% depth at the presumptive vitreoretinal border and 100% depth at the presumptive retina-choroid border. The present resolution is sufficient for extracting meaningful layer-specific anatomical and functional data, as previously discussed.[4,30]

Water Content MRI. In separate subgroups of C57BL/6 and 129S6/SvEvTac mice, six three-dimensional turbo-FLASH images were collected (Repetition time [TR], 1000 ms; matrix size, 160 × 320; Echo time [TE], 3.04 ms; Field-of-view [FOV], 8 × 8 mm^2; 16 slices, slice thickness, 600 μm; flip angle 3°; and the echo spacing [the time between pulses within a train] was 8.7 ms) such that a central slice was colocalized with the structure and diffusion-weighted (described above). The six images were registered (rigid-body) and averaged. These data represent proton density maps, which were converted into water content maps by normalizing to the vitreous as previously described and summarized below.[25] In a different subset of C57BL/6 and 129S6/SvEvTac mice, we collected proton density data in the dark and again at 13 minutes and 29 minutes (midpoints) after light exposure; these light data were averaged to estimate proton density at 21 minutes of light. As shown below, agreement across modalities and strains supports our use of the average apparent diffusion coefficient (ADC) and hydration data to represent the ∼20-minute light time point.

To convert the proton density in the outer retina into water content, we normalized it to 99% water content on either side

Investigative Ophthalmology & Visual Science

Downloaded from iovs.arvojournals.org on 04/21/2021

of the ONH (after correcting for the surface coil inhomogeneity and linearizing the retina[25]).[31] In addition, the intraretinal water profiles were adjusted to be a percentage of total retinal thickness for each animal (with 0% thickness at the vitreous-retinal border, and 100% thickness at the retina-choroid border); the depth into the retina of 80% to 100% was considered to be the posterior retina. The accuracy of using MRI to estimate retinal water content was confirmed previously by agreement between MRI-derived water content and specific gravity measurements.[25,32] We also previously validated the linearity of MRI signal intensity and water content in phantom studies.[25]

Diffusion MRI. In separate subgroups of mice, anatomic and apparent diffusion coefficient (ADC) MRI data sets were collected; the diffusion sensitizing gradient was set parallel to the optic nerve based on our previous observations that this is a useful direction for detecting changes in the outer retina.[3] In C57BL/6 mice, ADC was first acquired in the dark and then again 15 minutes after turning on the light; each ADC data set takes 10 minutes to collect, so we refer to the mi-point in the ADC collection as 20 minutes of light exposure. For 129S6/SvEvTac mice, we collected ADC data in the dark and again at 13 minutes and 29 minutes (midpoints) after light exposure for a different study. However, we also used the light data herein by averaging these time points to estimate the ADC at 21 minutes of light. Anatomic images were acquired using a spin-echo sequence (slice thickness, 600 μm; TR, 1000 ms; TE, 11 ms; matrix size, 192×320; field of view, 8×8 mm^2; number of acquisitions (NA), 2; axial resolution for central retina, 25 μm). Images sensitized to water diffusion were collected (TR, 1000 ms; slice thickness, 600 μm; TE, 33 ms; matrix size, 174×288; field of view, 8×8 mm^2; axial resolution for central retina, 27.8 μm; b = 0, 100, 250, 500, 600, 750, 990 s/mm^2 [collected in pseudo-random order, NA 1 per b value]), registered to the anatomic image, and analyzed (using in-house code) to generate ADC profiles from the central retina. We have previously established that the present resolution in the central retina is sufficient for extracting meaningful changes in central retinal thickness on the anatomic images and significant ADC changes at 88% to 100% depth, as previously discussed.[2,4,28] Data, largely free of choroidal contamination, were thus analyzed as described in detail in prior publications.[4]

Statistical Analysis

Seven mice from each strain were used, and three punches were taken from each retina in the seahorse experiment. All outcomes (OCT thickness, ADC, and water content) were measured multiple times within each animal. As such, we used linear mixed models to examine the differences between strains and between light exposures. A significance level of 0.05 was used for all analyses.

The model for OCT thickness included the fixed effects of strain and light exposure along with the interaction between strain and light exposure. This model also included the random effect of mouse within strain.

The relationship between ADC and retinal depth was modeled using restricted cubic splines for depth to compare mouse-specific profiles between groups. The number of "windows" with a relationship between ADC and retinal depth (i.e., "knots") was initially evaluated separately for each group for any given analysis, and the Akaike and Schwarz Bayesian information criteria (AIC and BIC, respectively) were used to identify the model with the fewest knots needed to model all groups, leading us to select six knots for the final model. Random coefficients for the intercept, light exposure, depth-specific coefficients (cubic spline coefficients), and interactions for light exposure/depth were also evaluated using AIC and BIC. The random coefficients for the intercept, light exposure, depth, the interaction between light exposure and depth, positive cubic distance of depth from knot 3, and positive cubic distance of depth from knot 4 were included in the final model. This model also included the fixed effects of strain, light exposure, location-specific values for the cubic splines, and all interactions among the main effects. The three-way interaction for strain/light-exposure/retinal depth was significant based on a likelihood ratio test ($P < 0.0001$). Given these results, we used the model with all three-way interactions in testing for differences between the strain/light-exposure groups. We used numeric integration to estimate the mean for any region identified as showing a response to light exposure.

We initially examined the relationship between water content and depth by using cubic splines for the entire retinal region. However, the mouse-specific water-depth profiles could not be fit well across the entire region using this approach. As such, we focused on the outer retina, with the relationship between water content and retinal depth being modeled using quadratic regression. Random coefficients for the intercept, light exposure, and depth (linear and quadratic coefficients), and interactions for light exposure/depth were evaluated using AIC and BIC. The random coefficients for the intercept, light exposure, depth, and the interaction between light exposure and depth were included in the final model. This model also included the fixed effects of strain, light exposure, depth, and all interactions among the main effects. The three-way interaction for strain/light-exposure/retinal depth was significant based on a likelihood ratio test ($P = 0.0461$). Thus, we included the interaction in testing for differences between strain/light-exposure groups. We used numeric integration to estimate the mean water content for any region identified as showing a response to light exposure.

Results

OCR and MRC

Light-adapted retina from C57BL/6 mice ex vivo displayed higher (13%, $P < 0.05$) basal OCR than that of 129S6/SvEvTac mice (Figs. 1A, 1C). Mitochondria content, as measured by pooled cytochrome *a* (cyt *a*) levels, was 8.85 pmol/retina in C57BL/6 mice and 10.81 pmol/retina in 129S6/SvEvTac mice; alternatively, cyt *a* content was 0.44 pmol (C57BL/6) and 0.54 pmol (129S6/SvEvTac) per retinal punch assayed. Normalizing the OCR data to the strain-specific cyt *a* quantity also revealed a higher (39%; $P < 0.01$) basal OCR level in C57BL/6 than 129S6/SvEvTac retina (Figs. 1B, 1C). In addition, mitochondria in C57BL/6 retina exhibited a smaller MRC value than that of 129S6/SvEvTac mice (Fig. 1D). Both normalized and unnormalized results suggest that mitochondria in the retina of C57BL/6 mice function at higher capacity and consume more oxygen. As water production is directly proportional to oxygen consumption, our data suggest that the retina (and thereby rod photoreceptors, which constitute almost 75% of all retinal cells) in C57BL/6 mice produce more water in light than 129S6/SvEvTac mice.[11]

Water Content MRI

The measurement of water content in vivo in C57BL/6 mice revealed that outer hydration was increased significantly ($P < 0.05$) with light exposure compared to that in darkness (Fig. 2). However, no light-evoked change in posterior retina hydration was noted in 129S6/SvEvTac mice (Fig. 2). Water content was not different in the dark between the two strains of mice but was different in the light (Fig. 2).

Investigative Ophthalmology & Visual Science

Downloaded from iovs.arvojournals.org on 04/21/2021

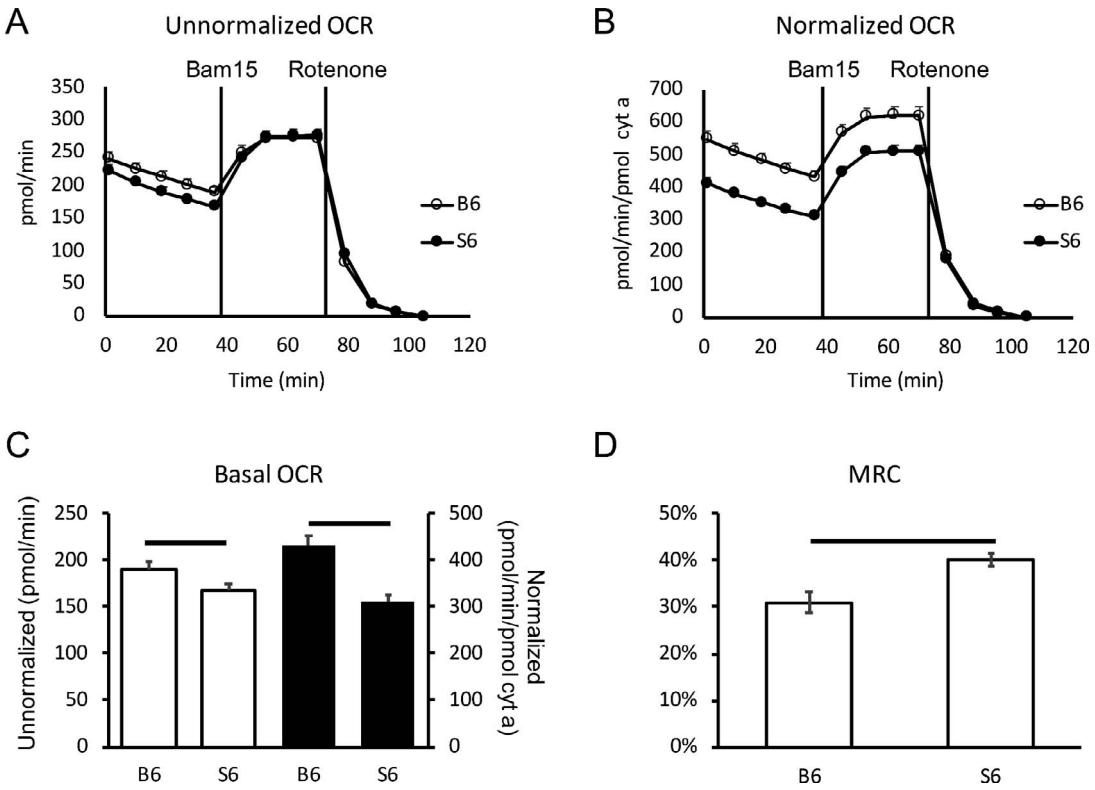

Figure 1. Basal OCR and MRC of C57BL/6 and 129S6/SvEvTac mouse retina. (**A**) Unnormalized OCR measurements in retinal punches from C57BL/6 (*open circle*) and 129S6/SvEvTac (*closed circle*) mice. (**B**) OCR after normalization to cyt *a* content in retinal punches. (**C**) Basal OCR level in C57BL/6 and 129S6/SvEvTac retinal punches. *Open bar* shows unnormalized and *black-filled bar* shows normalized values. (**D**) MRC in C57BL/6 and 129S6/SvEvTac retina. $n = 7$ for each group. *Error bar* indicates SEM. *Horizontal range bar* shows the region with significant differences ($P < 0.05$) between profiles.

Optical Coherence Tomography

Figure 3 shows examples of OCT images captured from the same eye under light- and dark-adapted conditions in a C57BL/6 mouse (left panel) and a 129S6/SvEvTac mouse (right panel). Light-adapted OCT images of C57BL/6 mice have an additional hyporeflection band between photoreceptor tip layer and RPE layer compared to the mice in the dark (Fig. 3). On the other

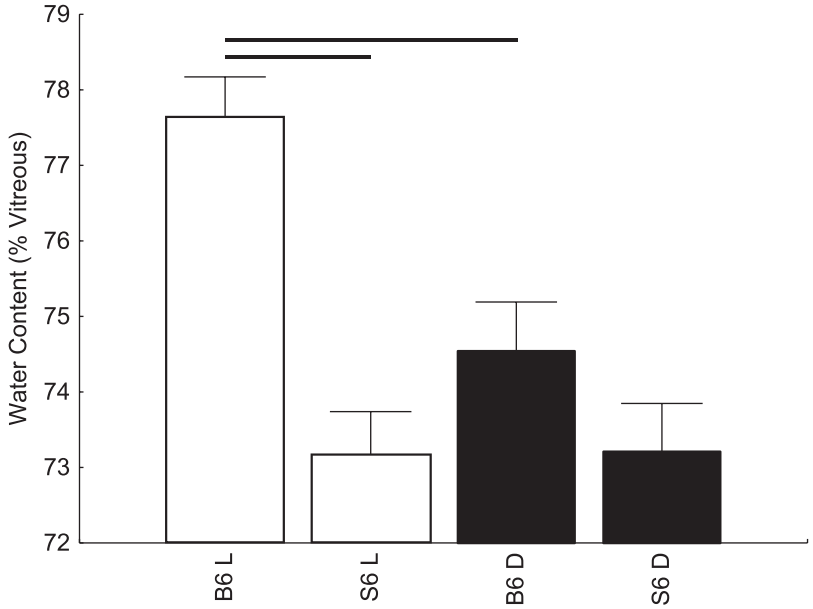

Figure 2. A summary of modeled central water content (as a percent of preretinal vitreous signal) in the posterior retina (80%–100% depth from the vitreoretina border) during dark (*closed symbols*) and at 20 to 21 minutes of ~500 lux light (*open symbols*). C57BL/6 ($n = 7$, dark; $n = 6$, light), and 129S6/SvEvTac ($n = 5$ dark-light pairs) mice. *Horizontal range bar* indicates the region with significant differences ($P < 0.05$) between profiles.

Investigative Ophthalmology & Visual Science

Downloaded from iovs.arvojournals.org on 04/21/2021

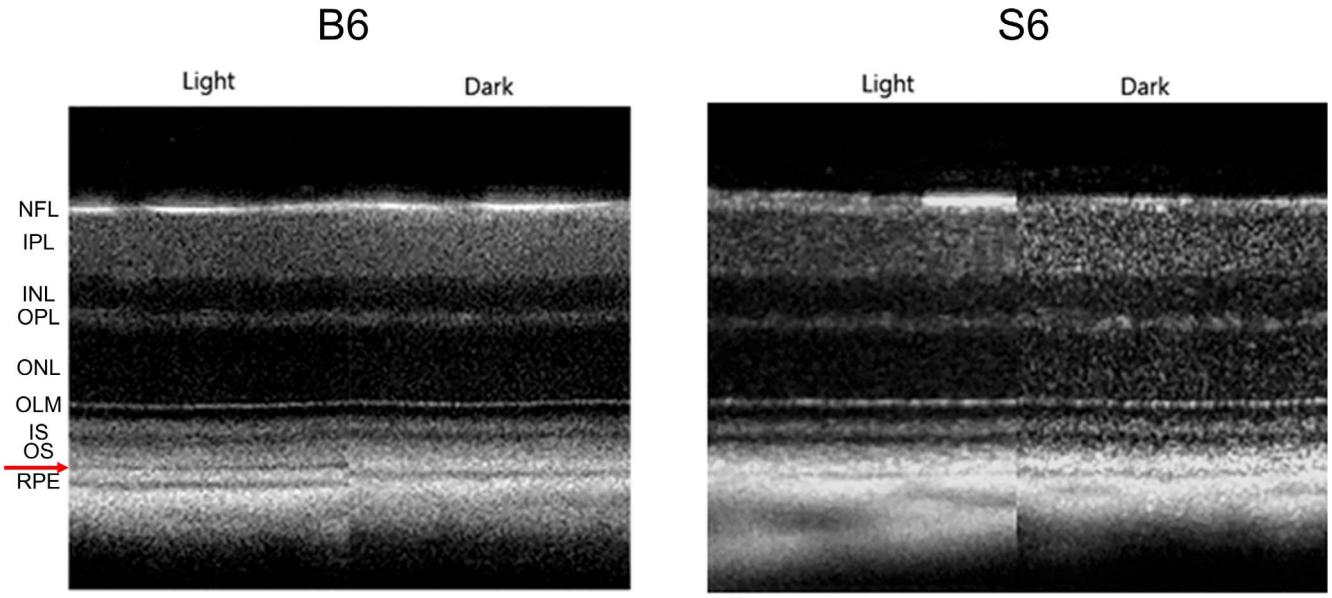

Figure 3. Representative same-eye OCT images in light and dark for C57BL/6 and 129S6/SvEvTac mice. Layer assignments are NFL, nerve fiber layer; INL, inner nuclear layer; IPL, inner plexiform layer; IS, rod inner segment layer; OLM, outer limiting membrane; ONL, outer nuclear layer; OPL, outer plexiform layer; OS, rod outer segment layer; and RPE, retinal pigment epithelium, as previously published.[47] *Red arrow* points to the hyporeflective band between the OS and RPE layer observed on the light-adapted OCT image of C57BL/6 mice.

hand, this hyporeflective band is not observed on light-adapted OCT images from 129S6/SvEvTac mice, and the photoreceptor tip layer is merged with RPE layer, a feature resembling OCT images from dark-adapted C57BL/6 mice (Fig. 3). In addition, light adaptation induced a relatively smaller increase in the thickness of the outer retina in 129S6/SvEvTac mice than in C57BL/6 mice (Fig. 4).[5]

Diffusion MRI

As shown in Figure 5, the posterior retina in C57BL/6 mice exhibited a significant ($P < 0.05$) increase in ADC relative to that in darkness, consistent with an increased outer retina volume/water mobility.[3,4] In contrast, ADC values in light were not significantly different from those in darkness at any location across the retina of 129S6/SvEvTac mice (Fig. 5).

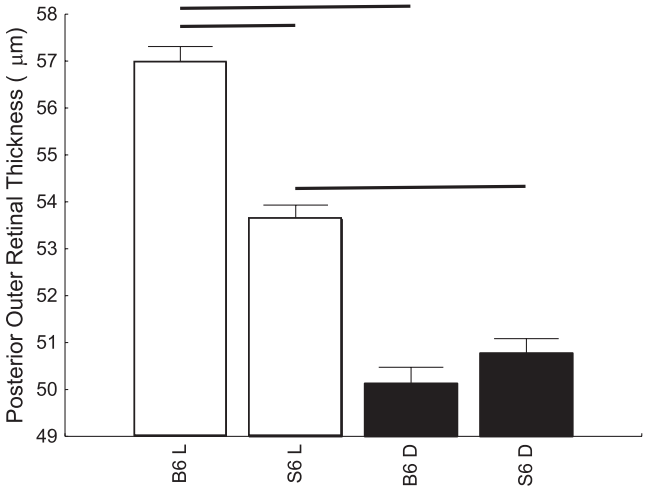

Figure 4. Summary of outer retina thickness, measured from OCT image in light and dark for C57BL/6 ($n = 7$) and 129S6/SvEvTac ($n = 8$) mice.

Discussion

In this study, we provide evidence for different outer retinal energy ecosystems in C57BL/6 and 129S6/SvEvTac mice, in agreement with less direct previous reports.[15–22] The differences in mitochondrial respiration suggested distinctions in strain-specific light-driven outer retina hydration in vivo, which we validated by using proton density MRI, ultrahigh-resolution OCT, and diffusion MRI.[3–11,27] Our results support the interpretation of the local light-driven imaging responses in

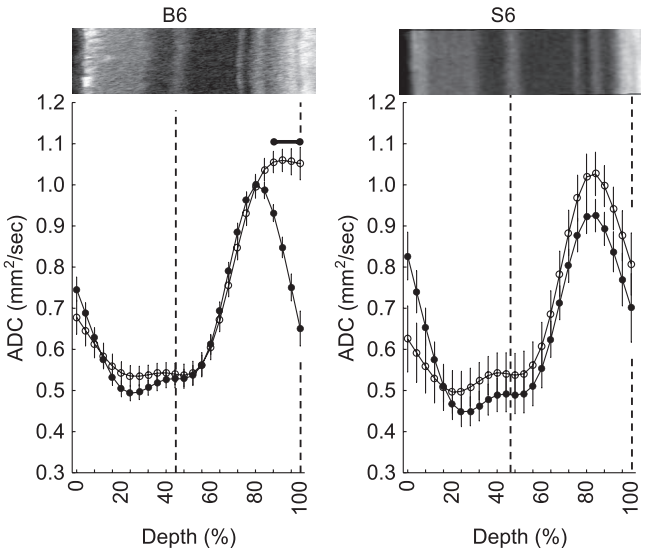

Figure 5. Summary of modeled central retinal ADC as a function of retinal depth during dark (*closed symbols*) and at 20 to 21 minutes of ~500 lux light (*open symbols*), in C57BL/6 ($n = 23$ dark-light pairs) and 129S6/SvEvTac mice ($n = 6$ dark-light pairs). *Horizontal range bar* indicates the region with significant differences ($P < 0.05$) between profiles. A representative OCT image (above profiles) is shown here. *Dashed vertical lines* map the outer plexiform layer and retina/choroid boundary onto diffusion profiles.

Downloaded from iovs.arvojournals.org on 04/21/2021

normal retina as a function of respiratory-induced hydration of the posterior retina. Based on these findings, we suggest that light-evoked imaging response in retinal disease, such as diabetic retinopathy, may be a biomarker of changes in mitochondrial activity, a previously understudied component of the light-based expansion of the outer retina.[4,6]

Some aspects of the experimental designs of the MRI and OCT arms of the study need comment. First, we did not find evidence that the anesthesia substantially altered the light-evoked expansion of the outer retina because, in this study, the effect was observed using two different anesthetics (urethane for the MRI studies and ketamine/xylazine for OCT); and, in our other studies, light-induced changes in the outer retina are also seen on OCT images of B6 mice anesthetized with isoflurane (data not shown). In addition, the light/dark order was not randomized because it takes several hours to fully dark adapt the retina. As previously shown, after light exposure, outer retinal changes on OCT return to initial values.[5]

The present study identifies strain differences in energy regulation and imaging responses to light. One contributing factor may be the established difference in rhodopsin regeneration rate in C57BL/6 and 129S6/SvEvTac mice as a consequence of having different RPE65 variants.[18] Notably, a previous study did not find evidence that the rate of rhodopsin regeneration per se contributes substantially to the light-evoked increases in posterior retinal thickness.[7] Another likely factor is that the 129S6/SvEvTac strain contains a natural mutation of the *DISC1* gene that prevents the production of the full-length protein, which plays an important role in regulating mitochondrial function in collaboration with the mitochondrial inner membrane protein mitofillin.[20] Deficiency in *DISC1* function has been reported to induce mitochondrial dysfunction, such as decreased NADH dehydrogenase activity, disrupted mitochondrial Ca^{2+} dynamics, reduction in mitochondrial monoamine oxidase activity, and reduced cellular ATP contents.[22] In this study, we observed higher basal OCR in C57BL/6 than 129S6/SvEvTac retina that is strongly weighted by a rod photoreceptor component. Our data thus suggest that mitochondria function more efficiently in C57BL/6 than in 129S6/SvEvTac retina. Additional studies are needed to explore a potential causal relationship between *DISC1* mutation in 129S6/SvEvTac mice and the observed difference in OCR and MRC compared to the other strain.[20,21]

C57BL/6 and 129S6/SvEvTac mice have been suggested to have distinct photoreceptor energy ecosystems in part because of different insult-induced morbidity outcomes.[19,33–35] The energy bionetwork is important in this regard because it regulates large light-driven swings in photoreceptor ATP production, which is required to support phototransduction and modify ion channel function and outer retina ion content.[19,36–44] In support of this view, mice genetically modified to prevent phototransduction exhibit no OCT and diffusion MRI responses.[4,7] The results presented here support this energy ecosystem concept, but additional work is needed to determine, for example, the differences in mitochondria morphology, density, or function between C57BL/6 and 129S6/SvEvTac mice.

The reasons for disparities between light-stimulated changes of outer retinal water content, retinal thickness, and water mobility indices are currently unclear. One possibility is that subtle alterations are more sensitively detected using OCT retinal thickness measurements compared with MRI assessment of proton density and water mobility. For example, 129S6/SvEvTac mice in this study show light-evoked expansion based on OCT retinal thickness (Fig. 4), but we are not able to detect such expansion using ADC MRI (Fig. 5). However, the extent of light-evoked expansion is less for 129S6/SvEvTac than for C57BL/6 mice by using both OCT retinal thickness and ADC MRI. The lack of a statistically significant expansion in 129S6/SvEvTac mice based on ADC MRI (Fig. 5) may be due to a lack of statistical power and perhaps lower resolution of this method. In addition, the posterior retina water content measured herein reflects the net result of water production minus water removal. An adult mammalian retina is estimated to generate, by aerobic respiration and glycolysis, 1.8 times more water in dark than in the light.[11] Rod photoreceptors being the most prevalent cell type are likely a major contributor to retinal water production.[45] Water removal in the outer retina is largely controlled by RPE pump activity.[11] Future studies could determine relative contributions of water production and removal in each strain studied herein. Nonetheless, all three imaging methods led to the same conclusion, that is 129S6/SvEvTac mice have a lower photoresponse in the outer retina than C57BL/6 mice.

MRI inherently measures the proton density associated with water, which is 110 M in equivalent protons. Proton density has been used to accurately assess retinal layer-specific water content after calibration against preretinal vitreous water signal.[25,31,32] This is an advance over conventional imaging methods, such as OCT, that noninvasively evaluates retinal thickness, but not water content directly.[25] Notably, MRI water content reflects a combination of intra- and extracellular hydration information because intracellular water resides in intracellular and extracellular compartments for short times (∼msec) relative to the time it takes to acquire an image (∼minutes).[46] Nonetheless, we previously observed an agreement between MRI and specific gravity measurements of retinal water content.[25]

In summary, the present results support and extend previous findings of parallels between light-stimulated ultra-high-resolution OCT and functional diffusion MRI responses. The data herein suggest that both methods assess the same phenomena, that is increased posterior retina hydration in light linked with mitochondrial respiration. Furthermore, these imaging responses are strongly regulated by the genetic background, a previously unappreciated modifier that needs to be considered in future studies of retinal diseases both in animal models and patients.

Acknowledgments

The authors thank Rod Braun, Ivy Samuels, and Raul Covian for helpful discussions and thank Raul Covian for cytochrome *a* measurements.

Supported by the National Institutes of Health (RO1 EY026584 and RO1 AG058171 to BAB; Intramural Research Programs EY000450 and EY000546 to AS; and EY000503 and EY000530 to HQ), NEI Core Grant P30 EY04068, and an unrestricted grant from Research to Prevent Blindness (Kresge Eye Institute).

Disclosure: **B.A. Berkowitz**, None; **R.H. Podolsky**, None; **H. Qian**, None; **Y. Li**, None; **K. Jiang**, None; **J. Nellissery**, None; **A. Swaroop**, None; **R. Roberts**, None

References

1. Swindell W, Ensrud K, Cawthon P, et al. Indicators of "Healthy Aging" in older women (65–69 years of age). A data-mining approach based on prediction of long-term survival. *BMC Geriatrics*. 2010;10:55.
2. Berkowitz BA, Bissig D, Roberts R. MRI of rod cell compartment-specific function in disease and treatment in-ávivo. *Prog Retin Eye Res*. 2016;51:90–106.
3. Bissig D, Berkowitz BA. Light-dependent changes in outer retinal water diffusion in rats in vivo. *Mol Vis*. 2012;18:2561–2577.

Investigative Ophthalmology & Visual Science

Downloaded from iovs.arvojournals.org on 04/21/2021

4. Berkowitz BA, Grady EM, Khetarpal N, Patel A, Roberts R. Oxidative stress and light-evoked responses of the posterior segment in a mouse model of diabetic retinopathy. *Invest Ophthalmol Vis Sci*. 2015;56:606–615.
5. Li Y, Fariss RN, Qian JW, Cohen ED, Qian H. light-induced thickening of photoreceptor outer segment layer detected by ultra-high resolution OCT imaging. *Invest Ophthalmol Vis Sci*. 2016;57:105–111.
6. Lu CD, Lee B, Schottenhamml J, Maier A, Pugh EN, Fujimoto JG. Photoreceptor layer thickness changes during dark adaptation observed with ultrahigh-resolution optical coherence tomography. *Invest Ophthalmol Vis Sci*. 2017;58:4632–4643.
7. Zhang P, Zawadzki RJ, Goswami M, et al. In vivo optophysiology reveals that G-protein activation triggers osmotic swelling and increased light scattering of rod photoreceptors. *Proc Natl Acad Sci U S A*. 2017;114:E2937–E2946.
8. Huang B, Karwoski CJ. Light-evoked expansion of subretinal space volume in the retina of the frog. *J Neurosci*. 1992;12:4243–4252.
9. Li JD, Govardovskii VI, Steinberg RH. Light-dependent hydration of the space surrounding photoreceptors in the cat retina. *Vis Neurosci*. 1994;11:743–752.
10. Govardovskii VI, Li JD, Dmitriev AV, Steinberg RH. Mathematical model of TMA+ diffusion and prediction of light-dependent subretinal hydration in chick retina. *Invest Ophthalmol Vis Sci*. 1994;35:2712–2724.
11. Adijanto J, Banzon T, Jalickee S, Wang NS, Miller SS. CO2-induced ion and fluid transport in human retinal pigment epithelium. *J Gen Physiol*. 2009;133:603–622.
12. Li JD, Gallemore RP, Dmitriev A, Steinberg RH. Light-dependent hydration of the space surrounding photoreceptors in chick retina. *Invest Ophthalmol Vis Sci*. 1994;35:2700–2711.
13. Uehara F, Matthes MT, Yasumura D, LaVail MM. Light-evoked changes in the interphotoreceptor matrix. *Science*. 1990;248:1633–1636.
14. Cooper RF, Tuten WS, Dubra A, Brainard DH, Morgan JIW. Non-invasive assessment of human cone photoreceptor function. *Biomed Opt Express*. 2017;8:5098–5112.
15. May-Simera H, Nagel-Wolfrum K, Wolfrum U. Cilia—the sensory antennae in the eye. *Prog Retin Eye Res*. 2017;60:144–180.
16. Wenzel A, Grimm C, Samardzija M, Remé CE. The genetic modifier Rpe65Leu 450 : effect on light damage susceptibility in c-Fos-deficient mice. *Invest Ophthalmol Vis Sci*. 2003;44:2798–2802.
17. Maeda A, Maeda T, Imanishi Y, et al. Retinol dehydrogenase (RDH12) protects photoreceptors from light-induced degeneration in mice. *J Biol Chem*. 2006;281:37697–37704.
18. Kolesnikov AV, Tang PH, Parker RO, Crouch RK, Kefalov VJ. The mammalian cone visual cycle promotes rapid M/L-cone pigment regeneration independently of the interphotoreceptor retinoid-binding protein. *J Neurosci*. 2011;31:7900–7909.
19. Berkowitz BA, Podolsky RH, Lenning J, et al. Sodium iodate produces a strain-dependent retinal oxidative stress response measured in vivo using QUEST MRI. *Invest Ophthalmol Vis Sci*. 2017;58:3286–3293.
20. Koike H, Arguello PA, Kvajo M, Karayiorgou M, Gogos JA. Disc1 is mutated in the 129S6/SvEv strain and modulates working memory in mice. *Proc Natl Acad Sci U S A*. 2006;103:3693–3697.
21. Muhlhans J, Brandstatter JH, Giessl A. The centrosomal protein pericentrin identified at the basal body complex of the connecting cilium in mouse photoreceptors. *PLoS One*. 2011;6:e26496.
22. Park Y-U, Jeong J, Lee H, et al. Disrupted-in-schizophrenia 1 (DISC1) plays essential roles in mitochondria in collaboration with mitofilin. *Proc Natl Acad Sci U S A*. 2010;107:17785–17790.
23. Kooragayala K, Gotoh N, Cogliati T, et al. Quantification of oxygen consumption in retina ex vivo demonstrates limited reserve capacity of photoreceptor mitochondria. *Invest Ophthalmol Vis Sci*. 2015;56:8428–8436.
24. Medrano CJ, Fox DA. Oxygen consumption in the rat outer and inner retina: light- and pharmacologically-induced inhibition. *Exp Eye Res*. 1995;61:273–284.
25. Berkowitz BA, Bissig D, Ye Y, Valsadia P, Kern TS, Roberts R. Evidence for diffuse central retinal edema *in vivo* in diabetic male Sprague Dawley rats. *PLoS One*. 2012;7:e29619.
26. Gerencser AA, Neilson A, Choi SW, et al. Quantitative microplate-based respirometry with correction for oxygen diffusion. *Anal Chem*. 2009;81:6868–6878.
27. Li Y, Zhang Y, Chen S, Vernon G, Wong WT, Qian H. Light-dependent OCT structure changes in photoreceptor degenerative rd 10 mouse retina. *Invest Ophthalmol Vis Sci*. 2018;59:1084–1094.
28. Bissig D, Berkowitz BA. Same-session functional assessment of rat retina and brain with manganese-enhanced MRI. *NeuroImage*. 2011;58:749–760.
29. Cheng H, Nair G, Walker TA, et al. Structural and functional MRI reveals multiple retinal layers. *Proc Natl Acad Sci U S A*. 2006;103:17525–17530.
30. Berkowitz BA, Grady EM, Roberts R. Confirming a prediction of the calcium hypothesis of photoreceptor aging in mice. *Neurobiol Aging*. 2014;35:1883–1891.
31. Aguayo J, Glaser B, Mildvan A, Cheng HM, Gonzalez RG, Brady T. Study of vitreous liquifaction by NMR spectroscopy and imaging. *Invest Ophthalmol Vis Sci*. 1985;26:692–697.
32. Stefansson E, Wilson CA, Lightman SL, Kuwabara T, Palestine AG, Wagner HG. Quantitative measurements of retinal edema by specific gravity determinations. *Invest Ophthalmol Vis Sci*. 1987;28:1281–1289.
33. Kanow MA, Giarmarco MM, Jankowski CS, et al. Biochemical adaptations of the retina and retinal pigment epithelium support a metabolic ecosystem in the vertebrate eye. *Elife*. 2017;6:e228899.
34. Zhou P, Kannan R, Spee C, Sreekumar PG, Dou G, Hinton DR. Protection of retina by αB crystallin in sodium iodate induced retinal degeneration. *PLoS One*. 2014;9:e98275.
35. Wang J, Iacovelli J, Spencer C, Saint-Geniez M. Direct effect of sodium iodate on neurosensory retina. *Invest Ophthalmol Vis Sci*. 2014;55:1941–1953.
36. Okawa H, Sampath AP, Laughlin SB, Fain GL. ATP consumption by mammalian rod photoreceptors in darkness and in light. *Curr Biol*. 2008;18:1917–1921.
37. Wangsa-Wirawan ND, Linsenmeier RA. Retinal oxygen: fundamental and clinical aspects. *Arch Ophthalmol*. 2003;121:547–557.
38. Zhang SB, Maguire D, Zhang M, et al. Mitochondrial DNA and functional investigations into the radiosensitivity of four mouse strains. *Int J Cell Biol*. 2014;2014:850460.
39. Danciger M, Matthes MT, Yasamura D, et al. A QTL on distal chromosome 3 that influences the severity of light-induced damage to mouse photoreceptors. *Mamm Genome*. 2000;11:422–427.
40. Cingolani C, Rogers B, Lu L, Kachi S, Shen J, Campochiaro PA. Retinal degeneration from oxidative damage. *Free Radic Biol Med*. 2006;40:660–669.
41. Johnson JE Jr, Perkins GA, Giddabasappa A, et al. Spatiotemporal regulation of ATP and Ca2+ dynamics in vertebrate rod and cone ribbon synapses. *Mol Vis*. 2007;13:887–919.
42. Linton JD, Holzhausen LC, Babai N, et al. Flow of energy in the outer retina in darkness and in light. *Proceed Natl Acad Sci*. 2010;107:8599–8604.

Investigative Ophthalmology & Visual Science

Downloaded from iovs.arvojournals.org on 04/21/2021

43. Wenzel A, Remé CE, Williams TP, Hafezi F, Grimm C. The Rpe65 Leu450Met variation increases retinal resistance against light-induced degeneration by slowing rhodopsin regeneration. *J Neurosci*. 2001;21:53–58.
44. Walsh N, Bravo-Nuevo A, Geller S, Stone J. Resistance of photoreceptors in the C57BL/6-c2J, C57BL/6J, and BALB/cJ mouse strains to oxygen stress: evidence of an oxygen phenotype. *Curr Eye Res*. 2004;29:441–447.
45. Jeon CJ, Strettoi E, Masland RH. The major cell populations of the mouse retina. *J Neurosci*. 1998;18:8936–8946.
46. Quirk JD, Bretthorst GL, Duong TQ, et al. Equilibrium water exchange between the intra- and extracellular spaces of mammalian brain. *Magn Reson Med*. 2003;50:493–499.
47. Berkowitz BA, Schmidt T, Podolsky RH, Roberts R. Melanopsin phototransduction contributes to light-evoked choroidal expansion and rod L-type calcium channel function in vivomelanopsin and choroid regulation. *Invest Ophthalmol Vis Sci*. 2016;57:5314–5319.

Investigative Ophthalmology & Visual Science

Downloaded from iovs.arvojournals.org on 04/21/2021